HTML ABSTRACT + LINKS

THE JOURNAL OF CHEMICAL PHYSICS **122,** 024307 (2005)

Close-coupling calculations of low-energy inelastic and elastic processes in ^{4}He collisions with H_2: A comparative study of two potential energy surfaces

Teck-Ghee Lee
Department of Physics and Astronomy, University of Kentucky, Lexington, Kentucky 40506, and Physics Division, Oak Ridge National Laboratory, Oak Ridge, Tennessee 37831

C. Rochow, R. Martin, T. K. Clark, and R. C. Forrey
Department of Physics, Penn State University, Berks-Lehigh Valley College, Reading, Pennsylvania 19610

N. Balakrishnan
Department of Chemistry, University of Nevada-Las Vegas, Las Vegas, Nevada 89154

P. C. Stancil
Department of Physics and Astronomy and Center for Simulational Physics, University of Georgia, Athens, Georgia 30602

D. R. Schultz
Physics Division, Oak Ridge National Laboratory, Oak Ridge, Tennessee 37831

A. Dalgarno
ITAMP, Harvard-Smithsonian Center for Astrophysics, Cambridge, Massachusetts 02138

Gary J. Ferland
Department of Physics and Astronomy, University of Kentucky, Lexington, Kentucky 40506

(Received 27 September 2004; accepted 25 October 2004; published online 21 December 2004)

The two most recently published potential energy surfaces (PESs) for the HeH_2 complex, the so-called MR (Muchnick and Russek) and BMP (Boothroyd, Martin, and Peterson) surfaces, are quantitatively evaluated and compared through the investigation of atom-diatom collision processes. The BMP surface is expected to be an improvement, approaching chemical accuracy, over all conformations of the PES compared to that of the MR surface. We found significant differences in inelastic rovibrational cross sections computed on the two surfaces for processes dominated by large changes in target rotational angular momentum. In particular, the $H_2(\nu=1,j=0)$ total quenching cross section computed using the BMP potential was found to be a factor of 1000 larger than that obtained with the MR surface. A lesser discrepancy persists over a large range of energies from the ultracold to thermal and occurs for other low-lying initial rovibrational levels. The MR surface was used in previous calculations of the $H_2(\nu=1,j=0)$ quenching rate coefficient and gave results in close agreement with the experimental data of Audibert *et al.* which were obtained for temperatures between 50 and 300 K. Examination of the rovibronic coupling matrix elements, which are obtained following a Legendre expansion of the PES, suggests that the magnitude of the anisotropy of the BMP potential is too large in the interaction region. However, cross sections for elastic and pure rotational processes obtained from the two PESs differ typically by less than a factor of 2. The small differences may be ascribed to the long-range and anharmonic components of the PESs. Exceptions occur for $(\nu=10,j=0)$ and $(\nu=11,j=1)$ where significant enhancements have been found for the low-energy quenching and elastic cross sections due to zero-energy resonances in the BMP PES which are not present in the MR potential. © *2005 American Institute of Physics.*
[DOI: 10.1063/1.1833351]

I. INTRODUCTION

The study of the He–H_2 interaction has a long history and can be traced back to at least the construction of a simple analytic potential energy surface (PES) by Roberts[1] in 1963. Since the beginning of the 1970s, scattering between atomic He and the H_2 molecule has been investigated experimentally.[2–4] The laser Raman scattering technique pioneered by Audibert *et al.*[3] has given accurate and detailed results. These experiments, which covered the sub-thermal regime, were accurate enough to reproduce the small structures in the measured rate constants (see Ref. 9) and have prompted considerable theoretical interest.[5–9] Calculations have been performed using *ab initio* and approximate quantal formalisms, classical and semiclassical methods, and various intermolecular potentials.

Collisions involving hydrogen molecules and helium atoms are of great interest for three main reasons. First, this collision system is a prototype for chemical dynamics studies and can be used as a testing ground for the scattering theory

 © 2005 American Institute of Physics

Downloaded 31 Dec 2004 to 146.186.234.236. Redistribution subject to AIP license or copyright, see http://jcp.aip.org/jcp/copyright.jsp

of nonreactive atom-diatom collisions involving a weak interaction potential. Second, rotational and vibrational transitions in H_2 induced by collisions with He are of practical importance in models of astrophysical environments where the physical conditions may not be accessible to terrestrial experiments. Examples include low densities characteristic of giant molecular clouds in the interstellar medium where star formation occurs. Heating of the interstellar cloud by strong shock waves induces rotational and vibrational excitation of the H_2 molecules leading to collision-induced dissociation to two free H atoms. Third, with recent experimental advances in the trapping of molecules,[10–13] collisional studies of the He–H_2 system have given new insight into the behavior of atom-diatom collisions at ultracold temperatures including investigations of Feshbach resonances, predissociation in van der Waals complexes, determination of complex scattering lengths, testing of effective range theory and Wigner threshold laws, and quasiresonant vibration-rotation energy transfer.[14–18]

Due to the continual advancement of computer technology and computational methodologies, theoretical studies[19,20] of inelastic collisions between He and H_2 have been performed with increasingly larger basis sets and have yielded a deeper understanding of the collision mechanism as well as providing benchmark data for astrophysics and chemistry. The accuracy of quantum scattering calculations is dictated by the flexibility and reliability of the interaction potential energy surface of the projectile atom and target diatom. Especially in the case of atom-diatom collisions in the ultracold regime, where the interaction time between the projectile atom and molecular target is considerably longer than the rotational/vibrational period of the molecule, the incoming atom is a sensitive probe of the PES of the complex. Consequently, the target molecule has time to adjust to the field of the slow moving atom and the scattering cross sections are sensitive to the anisotropy of the PES.

Muchnick and Russek[21] constructed a PES for He–H_2 which incorporated the *ab initio* potential energy calculations of Meyer *et al.*[22] and Russek and Garcia.[23] A crucial feature of Muchnick and Russek (MR) PES is the inclusion of the H_2 vibrational coordinate r to describe the motion of the nuclei in the molecule. The PES was constructed to behave in a physically realistic fashion in the nonequilibrium regions but the fit was not constrained by *ab initio* data.

The PES calculated by Muchnick and Russek was employed by Flower *et al.*[19] and later by Balakrishnan and co-workers,[15,20] and Forrey and co-workers[16–18] to obtain the cross sections and the corresponding rate coefficients for rovibrational transitions in ortho- and para-H_2 induced by collisions with He. Flower *et al.* applied a quantal coupled-channel method that used a harmonic oscillator approximation for the H_2 wave functions and their presented results for vibrational states $\nu=0$, 1, and 2. Comparison was made with previous calculations and with measurements at both low and high temperatures, and the agreement was found to be good. Balakrishnan *et al.*[15] performed similar calculations with numerically determined H_2 wave functions using Hermite basis sets and the H_2 potential of Schwenke.[24] Their predicted quenching rate coefficients with the MR PES gave good agreement with the experimental results of Audibert *et al.*[3] for vibrational relaxation of $H_2(\nu=1,j=0)$ by He impact at temperatures between 50 and 300 K. Subsequently, the same PES has been employed to investigate rotational and vibrational excitation transitions.[16–18,20]

The most recent analytic HeH_2 PES was constructed by Boothroyd, Martin, and Peterson (BMP) (Ref. 25) from more than 25 000 *ab initio* data points. The BMP surface not only accurately represents the van der Waals potential well, but also fits the interaction region with chemical accuracy, giving an order of magnitude improvement in *RMS* errors compared to the MR PES. While such an improvement is critical for chemical dynamics studies, the BMP potential was also constrained by the *ab initio* data to accurately describe large H_2-molecule sizes and short He impact distances. These enhancements allow studies of highly excited H_2 and collision-induced dissociation.

In this paper we present a comparative study of the MR and BMP potential surfaces for collisions of vibrationally and rotationally excited H_2 by He impact. The scattering cross sections and their corresponding rate coefficients are calculated using the nonreactive quantum mechanical close-coupling method. In Sec. II, we outline close-coupling theory and give a brief description of the PESs. We present our results and discussion in Sec. III and a summary and conclusion in Sec. IV. Atomic units are used throughout, unless otherwise noted, i.e., $e=m_e=a_o=1$ a.u., while 1 hartree $=27.2116$ eV $=627.51$ kcal/mol.

II. THEORETICAL METHODS

A. The close-coupling approach

Calculations of rovibrational transition cross sections and thermally averaged rate coefficients provide stringent tests of the potential energy surfaces of the HeH_2 molecule. To compute these cross sections and rate coefficients, we use a quantum-mechanical close-coupling method that has been described in detail elsewhere.[26] Here we provide a brief overview of the essential elements of the approach. The time-independent Schrödinger equation for the He+H_2 collision system in the center of mass frame is given by

$$(T_r+T_R+v_{H_2}(r)+V_I(r,R,\theta)-E)\Psi^{JM}(\vec{R},\vec{r})=0, \qquad (1)$$

with $T_r=-1/2m\nabla_r^2$ and $T_R=-1/2\mu\nabla_R^2$, where m is the reduced mass of the H_2 molecule and μ is the reduced mass of the He–H_2 complex. The internuclear distance between the two H atoms is denoted by r, R is the distance between the He atom and the center of mass of H_2, and θ is the angle between $\vec{r}$ and $\vec{R}$. The term $v_{H_2}(r)$ is the isolated H_2 potential and $V_I(r,R,\theta)$ is the He–H_2 interaction energy. To solve Eq. (1), we expand the total wave function $\Psi^{JM}(\vec{R},\vec{r})$ in the form

$$\Psi^{JM}(\vec{R},\vec{r})=\frac{1}{R}\sum_n C_n(R)\phi_n(\hat{R},\vec{r}), \qquad (2)$$

where the channel function $[n\equiv(\nu jl;JM)]$ is given by

Downloaded 31 Dec 2004 to 146.186.234.236. Redistribution subject to AIP license or copyright, see http://jcp.aip.org/jcp/copyright.jsp

$$\phi_n(\hat{R},\vec{r}) = \frac{1}{r}\chi_{\nu j}(r) \times \sum_{m_j,m_l} (j,l,J|m_j,m_l,M) Y^j_{m_j}(\hat{r}) Y^l_{m_l}(\hat{R}). \quad (3)$$

The vibrational and rotational quantum numbers are denoted by ν and j, respectively, and l is the orbital angular momentum of He with respect to H_2, J is the total angular momentum quantum number (i.e., $\vec{J}=\vec{l}+\vec{j}$), M is the projection of J onto the space-fixed z axis, and $(j,l,J|m_j,m_l,M)$ denotes a Clebsch-Gordon coefficient. The corresponding eigenvalues $\epsilon_{\nu j}$ (rovibrational binding energies) are obtained by solving the radial (r) nuclear Schrödinger equation for the diatom H_2,

$$\left(-\frac{1}{2m}\frac{d^2}{dr^2} + \frac{j(j+1)}{2mr^2} + v_{H_2}(r)\right)\chi_{\nu j}(r) = \epsilon_{\nu j}\chi_{\nu j}(r), \quad (4)$$

by expanding $\chi_{\nu j}(r)$ in terms of a Hermite polynomial basis with the H_2 potential $v_{H_2}(r)$, taken from Schwenke.[24] Substituting Eqs. (2)–(4) into Eq. (1), we arrive at a system of close-coupling equations

$$\left(\frac{d^2}{dR^2} - \frac{l_i(l_i+1)}{R^2} + 2\mu E_i\right) C_i(R) = 2\mu \sum_n C_n(R) \langle \phi_i | V_I | \phi_n \rangle, \quad (5)$$

where $E_i = E_{\nu j}$ is the initial kinetic energy and l_i is the orbital angular momentum in the ith channel. To solve the coupled radial equations (5), we used the hybrid modified log-derivative-Airy propagator[27] in the general purpose scattering code MOLSCAT.[28] The log-derivative matrix[27] is propagated to large intermolecular separations where the numerical results are matched to the known asymptotic solutions to extract the physical scattering matrix. This procedure is carried out for each partial wave until a converged cross section is reached. We have checked that the results are converged with respect to the number of partial waves as well as the matching radius for all channels included in the calculations.

We also adopt here the total angular momentum representation introduced by Arthurs and Dalgarno[29] in which the cross section for transitions from an initial νj vibrational-rotational level to the final $\nu' j'$ level is given by

$$\sigma_{\nu j \to \nu' j'}(E_{\nu j}) = \frac{\pi}{2\mu E_{\nu j}(2j+1)} \sum_{J=0}^{\infty} (2J+1) \times \sum_{l=|J-j|}^{|J+j|} \sum_{l'=|J-j'|}^{|J+j'|} |\delta_{jj'}\delta_{ll'}\delta_{\nu\nu'} - S^J_{jj'll'\nu\nu'}|^2. \quad (6)$$

The total energy E is related to the kinetic energy of the incoming particle according to $E = E_{\nu j} + \epsilon_{\nu j}$.

The rate coefficient for a given transition is obtained by averaging the appropriate cross section over a Boltzmann distribution of velocities of the projectile atom at a specific temperature T:

$$k_{\nu j \to \nu' j'}(T) = G \int_0^\infty dE_{\nu j} \sigma_{\nu j \to \nu' j'}(E_{\nu j}) E_{\nu j} e^{(-\beta E_{\nu j})}, \quad (7)$$

where the constant $G = \sqrt{(8/\mu\pi\beta)}\beta^2$ and $\beta = (k_B T)^{-1}$ with k_B being Boltzmann's constant. The total quenching rate coefficient can be calculated from

$$k_{\nu j}(T) = \sum_{\nu' j'} k_{\nu j \to \nu' j'}(T). \quad (8)$$

B. Potential energy surfaces of HeH_2

Being one of the simplest triatomic molecular systems, the HeH_2 PES has been extensively studied theoretically over the last four decades. Since each of He and H_2 has only two valence electrons in closed shells, this trimer provides a fundamental test of the quantum chemistry methods for calculating the van der Waals interactions. The search for evidence of a bound HeH_2 halo molecule is also a fascinating subject and its stability depends sensitively on the PES. The PES has also been explored experimentally using a variety of state-of-the-art experimental techniques.[30,31]

The historical development of the refinements of the HeH_2 PES, which can be traced back to at least the early 1960s, has been reviewed by BMP.[25] Here, we outline some characteristics of the two most recently published *ab initio* analytic HeH_2 potential energy surfaces, both of which we have incorporated into our scattering theory computer program. The first PES we used was published in 1994 by MR which was adopted in the scattering calculations performed by Flower *et al.*,[19] Balakrishnan and co-workers[15,20] and Forrey and co-workers.[16–18] This *ab initio* HeH_2 PES overcame many of the deficiencies of earlier PESs which adopted the rigid rotor approximation or considered only equilibrium H_2 geometries. These earlier PESs also lacked fits, either semi-empirical or empirical, for the remainder of the surface that was not constrained with *ab initio* data, which severely limited their use for atom-diatom collision calculations. However, MR generalized the HeH_2 PES based on the physics underlying the principal interaction mechanisms responsible for the PES, using 19 fitting parameters. This surface was fitted to a combination of the *ab initio* energies of Meyer *et al.*[22] and of Russek and Garcia.[23] As a result, the MR HeH_2 interaction was constructed to be accurate in the van der Waals potential well and at the small-R repulsive wall, and to have physically reasonable behavior in regions of the PES not constrained by *ab initio* data.

The second HeH_2 PES we employed is the most recent one published by Boothroyd *et al.*[25] in 2003. This PES was devised to represent accurately the van der Waals well and the interaction region required for chemical reaction dynamics. Consequently, a set of over 25 000 *ab initio* points was calculated for HeH_2 geometries. Both the ground-state and a few excited-state energies were computed, and the conical intersection of the ground state with the first excited state was mapped out approximately. A different analytic PES was fitted to the *ab initio* data, yielding an improvement by more than an order-of-magnitude in the fit in the interaction re-

Downloaded 31 Dec 2004 to 146.186.234.236. Redistribution subject to AIP license or copyright, see http://jcp.aip.org/jcp/copyright.jsp

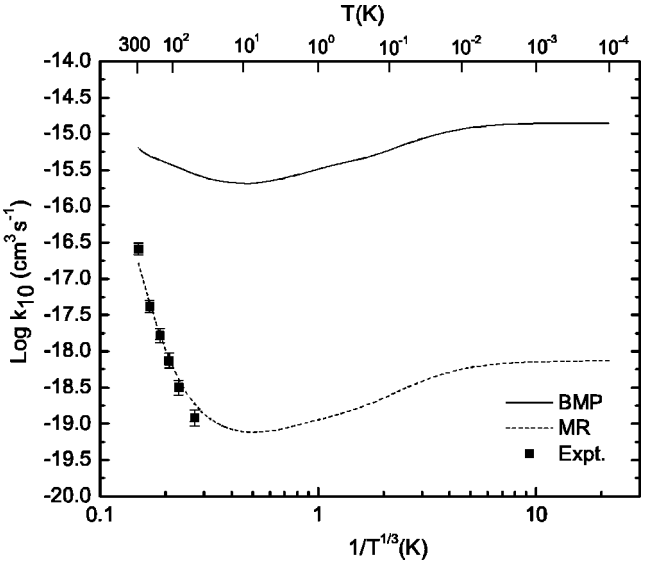

FIG. 1. Total quenching rate coefficient for $(v=1,j=0)$ as a function of temperature. The solid and dashed curves are results obtained using the BMP and MR potentials, respectively. The solid squares with error bars are the experimental results of Audibert *et al.* (Ref. 3). The MR curve agrees very well with the experimental data, whereas the BMP curve does not.

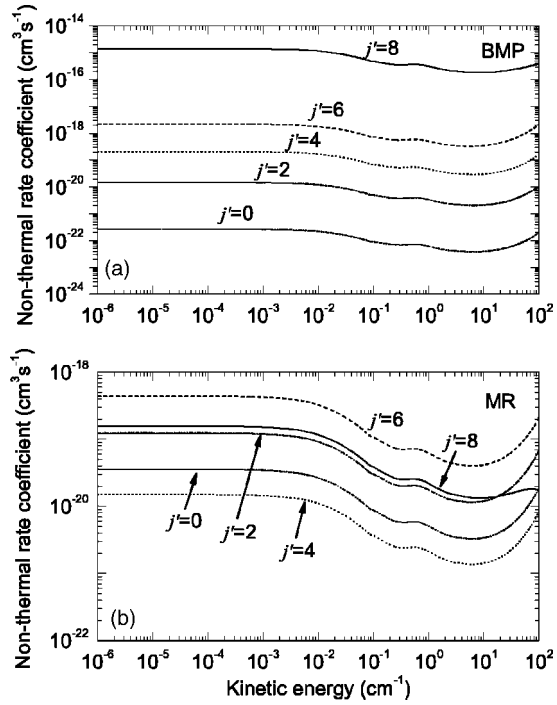

FIG. 2. Inelastic cross section $\sigma_{1,0\to 0,j'}$ times collision velocity (nonthermal rate coefficient) as a function of collision energy. Computed using the BMP (a) and MR (b) PES. The $j'=8$ contribution strongly dominates the BMP results over the entire energy range shown, and is responsible for the large discrepancy with experiment (see Fig. 1).

gion, compared to the MR HeH_2 PES. Unlike the MR PES, *ab initio* points were used to constrain the fit for large H–H separations.

Both the BMP and MR PESs are expressed as a function of distances between the three atoms in the system. For the purpose of the collision calculations, however, it is more convenient to expand the interaction potential in terms of Legendre polynomials P_λ of the order of λ as in the MOLSCAT computer program,

$$V_I(\vec{r},\vec{R})=\sum_{\lambda}^{\infty} v_\lambda(r,R)P_\lambda(\cos\theta). \tag{9}$$

The reduced potential coupling matrix elements required for the scattering calculations are obtained from

$$v^{\lambda}_{vj\to v'j'}(R)=\int_0^\infty dr\chi^*_{vj}(r)v_\lambda(r,R)\chi_{v'j'}(r). \tag{10}$$

Neither BMP nor MR express their PES functions in the form of Eq. (9), but in terms of multibody expansions with physically-motivated functional forms.

III. RESULTS AND DISCUSSION

We have carried out close-coupling calculations for collisions of ^{4}He with H_2 using the BMP and MR PESs. The total quenching rate coefficient for $H_2(v=1,j=0)$ is shown in Fig. 1 for temperatures in the range 10^{-4} K and 300 K. The rate coefficients attain finite values for temperatures lower than 1 mK in accordance with Wigner's law. Unexpectedly, we find that the total quenching rate coefficient computed with the BMP PES is as much as three orders of magnitude larger than that calculated with the PES of MR. Only the results from the MR PES agree with the experimental data of Audibert *et al.*[3] Good agreement with the Audibert *et al.* results were previously obtained by Balakrishnan *et al.*[15] who also used the MR PES. This significant discrepancy suggests that the PES of BMP may contain some unphysical behavior in either the newly computed *ab initio* data or the adopted fit functions. The different slopes of the rate coefficients obtained using the BMP and MR surfaces indicate that a much larger fraction of the available energy is taken up as rotation in collisions on the BMP surface. To identify the origins of this discrepancy in the BMP surface, we have examined the constituent channels of the quenching rate coefficients.

Figure 2 displays the inelastic rovibrational state-to-state, nonthermal rate coefficients as a function of collision energy. The nonthermal rate coefficient is defined here as cross section $\sigma_{1,0\to 0,j'}$ times collision velocity v in the center of mass frame. The rate coefficients computed using the BMP PES [see Fig. 2(a)] are seen to increase monotonically with j' over the entire energy range. This behavior is in sharp contrast to the state-to-state rate coefficients computed with the MR surface shown in Fig. 2(b), which displays no obvious ordering with j'. The discrepancy between the total quenching rate coefficients shown in Fig. 1 is evidently due to the $j'=8$ channel with the BMP surface, the rate coefficient of which is more than three orders of magnitude larger than any of the state-to-state MR rate coefficients given in Fig. 2(b). An appreciable contribution also comes from the $j'=6$ channel with the BMP result being a factor of 10 larger than that obtained with the MR PES.

By calculating the λ-dependent potential couplings on Eq. (9), we may gain some insight into the origin of the discrepancies. Figure 3 shows diagonal and off-diagonal reduced potential coupling matrix elements, defined in Eq.

Downloaded 31 Dec 2004 to 146.186.234.236. Redistribution subject to AIP license or copyright, see http://jcp.aip.org/jcp/copyright.jsp

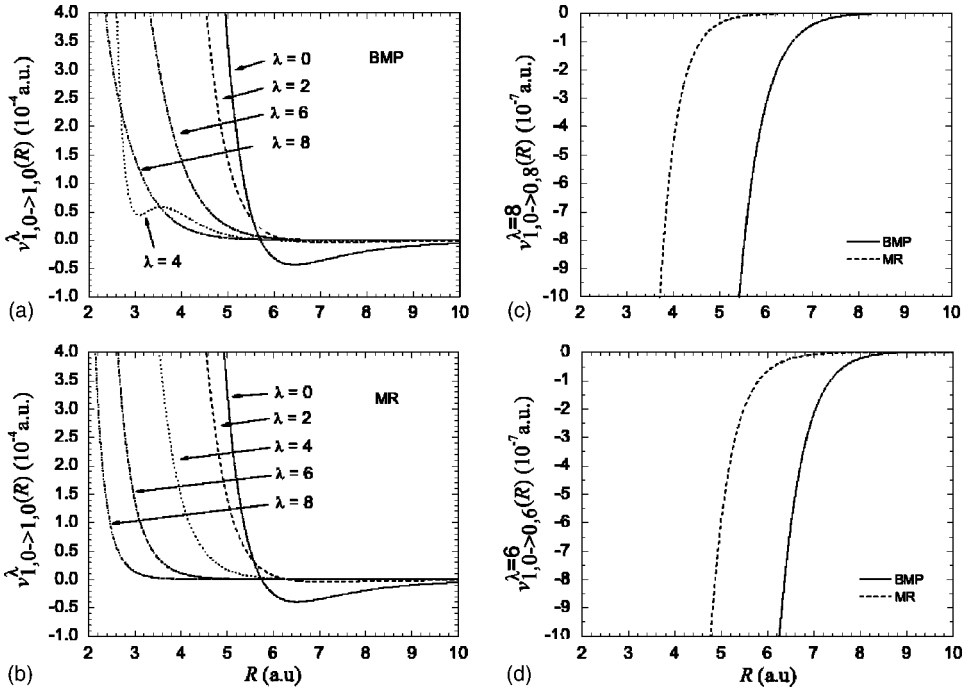

FIG. 3. (a) Diagonal matrix element for ($\nu=1,j=0$) using the BMP potential. The curves correspond to the $\lambda=0,2,4,6,8$ terms of a Legendre expansion of the potential energy surface [see Eq. (10)]. (b) Same as (a) but using the MR potential. (c) Off-diagonal coupling matrix element for $\lambda=8$. (d) Off-diagonal coupling matrix element for $\lambda=6$.

(10). Only the even terms contribute here since the diatom is a homonuclear molecule. To analyze the present results, which depend primarily on the intermediate and long-range behavior of the PES, we examine the first five terms ($\lambda=0$, 2, 4, 6, 8) in the expansion of $V_I(\vec{r},\vec{R})$. Figures 3(a) and 3(b) show a comparison between the BMP and MR diagonal matrix elements for ($\nu=1,j=0$). The first radial coefficient $v^0(R)$ represents the spherical component of the interaction, while the higher terms define the anisotropic behavior of the PES. Comparing $v^0(R)$ obtained from the BMP and MR PES, we find that the two yield essentially identical results with the repulsive wall of the ($\nu=1,j=0$) channel for both cases occurring at distances just less than $R=6$ a.u. While there are evidently significant differences for the higher $v^\lambda(R)$ terms for $R<5$ a.u., these differences appear inside the repulsive barrier [the $v^0(R)$ term], a region which will not be accessible in the low-energy collisions considered here, and therefore will have negligible impact on the cross sections.

In Figs. 3(c) and 3(d), the off-diagonal coupling matrix elements for the dominant state-to-state transitions obtained with the BMP surface are presented. Figure 3(c) reveals the striking difference between the BMP and MR off-diagonal coupling matrix element for $\lambda=8$. Comparing $\lambda=0$ of Fig. 3(a) with Fig. 3(c), we see that the BMP potential provides a significant off-diagonal $\lambda=8$ coupling for distances outside the potential barrier which are accessible during the collision. Conversely, the MR coupling is shifted to smaller R so that the magnitude of the coupling is significantly smaller in the interaction region. Therefore, the discrepancy in the $(1,0)\rightarrow(0,8)$ quenching rate coefficient, as well as the total, can be attributed to the enhancement by the BMP surface of the $\lambda=8$ off-diagonal coupling. Figure 3(d) makes a similar comparison of off-diagonal couplings for $\lambda=6$. The BMP coupling is again larger, but the difference is not as dramatic as for the $\lambda=8$ case consistent with the smaller differences between the $(1,0)\rightarrow(0,6)$ transition rate coefficients shown in Fig. 2.

The importance of including higher-order terms in the Legendre polynomial expansion of the interaction potential in accurately determining vibrational quenching rate coefficients at low temperatures has been the topic of a number of recent investigations.[32–35] Krems[32] showed that for the vibrational relaxation of CO($\nu=1$) by collisions with He atoms terms as high as $\lambda=30$ were required in Eq. (9) to obtain converged cross sections. In subsequent calculations, Krems *et al.*[33] reported similar behavior for the vibrational quenching of HF($\nu=1,j=0$) by collisions with Ar atoms which preferentially populate high-lying rotational levels in the $\nu=0$ vibrational level. In a more recent study Uudus *et al.*[34] reported significant differences in the low-temperature vibrational relaxation rates of $H_2(\nu=1,j=0)$ by collisions with Ar atoms computed using two different interaction potentials. They found that $(1,0)\rightarrow(0,8)$ transition dominates the quenching when the Ar–H_2 potential of Bissonnette *et al.*[36] is used, while no such preference is observed when the interaction potential of Schwenke *et al.*[37] is employed. As in the present study, the differences were attributed to enhanced off-diagonal coupling arising from the $\lambda=8$ term of the potential surface of Bissonnette *et al.*[36]

The dominance of the $(1,0)\rightarrow(0,8)$ transition found using the BMP PES is a consequence of two characteristics: (i) the small energy gap between the initial and final states (the energy gap is only 111 cm^{-1}) and (ii) the relatively large potential coupling shown in Fig. 3(c). In previous studies using the MR potential (i) was satisfied, but not (ii) so that the importance of this channel was not seen. Using the BMP potential, we can demonstrate that both characteristics are required to obtain a large transition rate by artificially enlarging the energy gap by increasing the target molecular re-

Downloaded 31 Dec 2004 to 146.186.234.236. Redistribution subject to AIP license or copyright, see http://jcp.aip.org/jcp/copyright.jsp

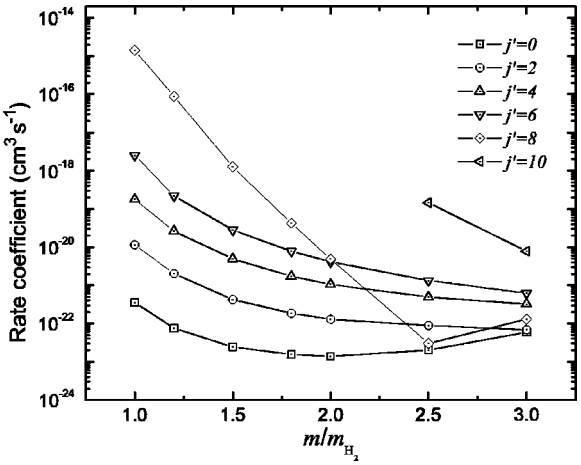

FIG. 4. Zero-temperature rate coefficients for $(\nu=1,j=0)$ as a function of diatom reduced mass m using the BMP potential. The nearly exponential behavior of the $j'=8$ contribution is consistent with exponential energy gap behavior seen previously.[17] The inelastic results for m corresponding to DT and T_2 are not as sensitive to the $j'=8$ contribution.

duced mass. In Fig. 4, the zero-temperature rate coefficient for the $(1,0)\rightarrow(0,j')$ transitions obtained with the BMP potential are displayed as a function of target molecule reduced mass. The nearly exponential decrease in the $(1,0)\rightarrow(0,8)$ transition, and the smaller decreases in the other channels, is consistent with the above argument. While there is no change in the BMP potential coupling, (i) is reduced with the increasing energy gap (increasing reduced mass) until the $(1,0)\rightarrow(0,8)$ channel loses its dominance for $m/m_{H_2}>2$. For $m/m_{H_2}\sim 2.5$ (where 2.4 corresponds to DT), the $j'=10$ channel becomes exoergic and its dominance is likely to be due to an enhanced BMP off-diagonal coupling for $\lambda=10$.

To ascertain whether the above discrepancy will manifest itself for other inelastic transitions, we also calculated the nonthermal rate coefficients for quenching of the initial $(\nu=2,j=0)$ state to individual rotational levels of the $\nu=1$ vibrational state using both the BMP and MR potential surfaces shown in Fig. 5. The dependence on j' of the transitions is identical to that seen for the $(\nu=1,j=0)$ quenching rate coefficients for the two potentials. Again, the major contribution comes from the $j'=8$ channel when the BMP potential is used.

For the higher vibrational states, we illustrate in Figs. 6(a) and 6(b) the variation of the total quenching rate coefficients with respect to the vibrational quantum number ν for $j=0$ and $j=1$ at zero temperature. We found that the $j'=8$ component is unmistakably dominant for $\nu<4$ when the BMP PES is used. However, when $\nu>4$, the $j'=8$ channel is closed and the total quenching rate is dominated by the $j'=6$ contribution. The peak observed at $\nu=10$ is due to a zero-energy resonance which is a consequence of a quasibound state of the HeH_2 complex (see below).

For $j=1$, shown in Fig. 6(b), there is no $j'=8$ contribution since transitions to this state are forbidden and there are no $j'=9$ contributions because the channel is closed for all ν. The major contribution to the total quenching rate coefficients comes from the $j'=7$ component $(\lambda=6)$ instead. We found that the $j'=7$ contribution for $j=1$ continues to be

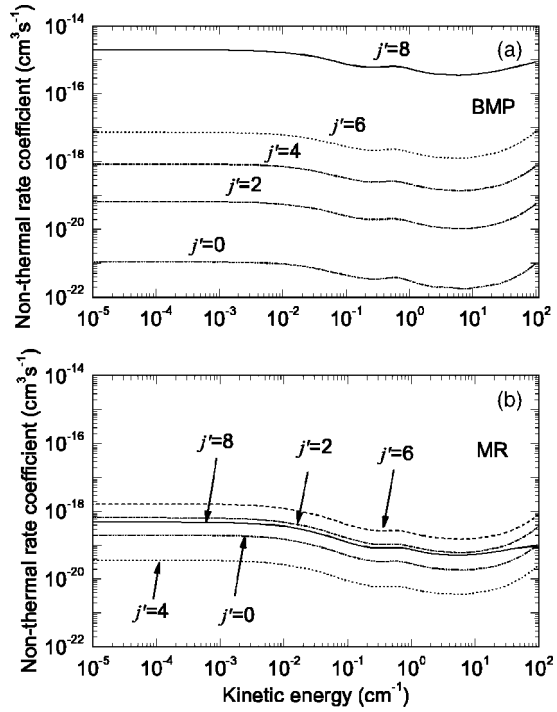

FIG. 5. Inelastic cross section $\sigma_{2,0\rightarrow 1,j'}$ times collision velocity (nonthermal rate coefficient) as a function of collision energy computed with the BMP (a) and the MR (b) potential. The $j'=8$ contribution again strongly dominates the BMP results and produces a significant disagreement with the MR results.

strong up to high energies; the zero-energy resonance is also present in the BMP PES for $\nu=11,j=1$.

In Figs. 7(a), 7(b), 8(a), and 8(b) we illustrate the energy-dependent elastic cross sections for $\nu=0$, 1, 2, and 10, respectively, for both the MR and BMP potentials and with $j=0$. The differences seen for the first three are likely due to improvements in the long-range portion of the BMP potential compared to that of the MR surface where anisotropy effects do not play a role. The two potentials give good agreement for elastic scattering at high collision energies.

For the $(\nu=10,j=0)$ elastic cross section, the results based on the two PESs give reasonable agreement at high collision energies. However, as the collision energy decreases below $E\sim 0.1\ \mathrm{cm}^{-1}$, the two curves start to deviate considerably. Both a significant enhancement of the elastic cross section with decreasing collision energy and a shift in the onset of the Wigner threshold behavior in the ultracold region can be attributed to the presence of a zero-energy resonance in the BMP PES-based calculation. This situation, where one PES-based calculation predicts a zero-energy resonance and the other does not, was seen before in the case of $Ar+H_2$ collisions.[38] Because the van der Waals potential well supports a weak quasibound state for each excited level of the diatom,[16] a small change in the PES can easily move the quasibound state into coincidence with the corresponding diatomic energy level. Therefore, the existence or absence of such a resonance is a very sensitive test of the details of the PES.

Returning to inelastic collisions, other differences that are manifested may be seen by considering the $\nu=10,j=0$

Downloaded 31 Dec 2004 to 146.186.234.236. Redistribution subject to AIP license or copyright, see http://jcp.aip.org/jcp/copyright.jsp

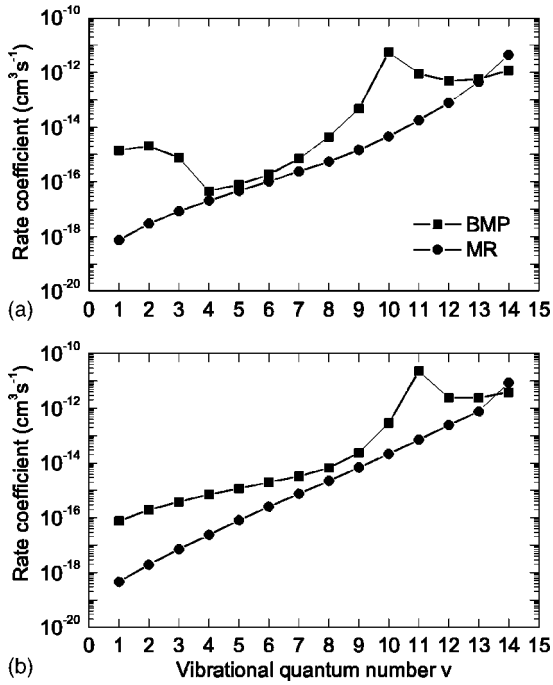

FIG. 6. (a) Zero-temperature total quenching rate coefficients for $j=0$ as a function of ν. The $j'=8$ contribution is strongly dominant for $\nu<4$ when using the BMP potential. For $\nu>4$, the $j'=8$ channel is closed and the total quenching rate is dominated by the $j'=6$ contribution. (b) Same as (a) but for $j=1$ case. The $j'=7$ contribution is dominant for low ν when using the BMP potential. The peaks in the BMP curves at $(\nu=10,j=0)$ and $(\nu=11,j=1)$ are due to zero-energy resonances. The influence of the zero-energy resonances disappears as the collision energy is increased. The large differences between the two potentials at low ν, however, persist for all energies.

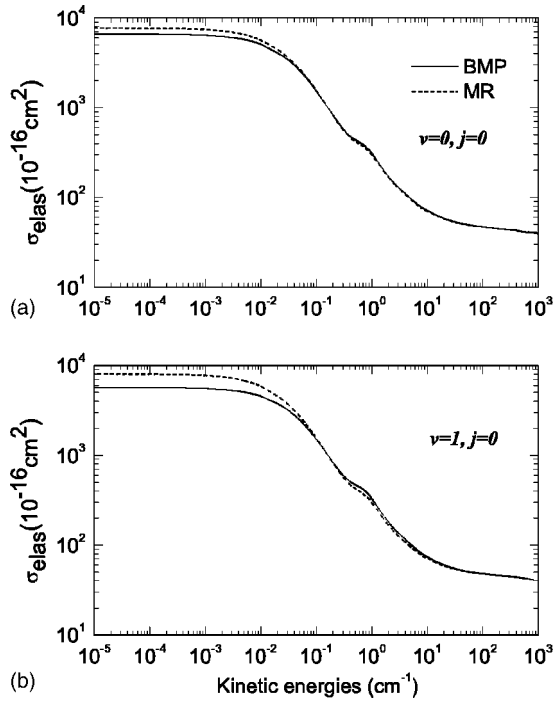

FIG. 7. Elastic cross sections $\sigma_{0,0}$ (a) and $\sigma_{1,0}$ (b) as a function of collision energy. The two potentials give good agreement for elastic scattering at high collision energies. The difference at ultracold energies is within a factor of 2, which is typical for most of the (v,j) levels of this system.

state since a peak in the ν distribution for the zero-energy quenching rate coefficient is evident in Fig. 6(a). Specifically, Figs. 9(a) and 9(b) show the energy dependence of the rate coefficients for transitions from the initial $(\nu=10,j=0)$ level into $(\nu=9,j')$ for the BMP and MR potentials, respectively. Figure 9(a) shows that for collision energies less than $\sim 0.1\ \mathrm{cm}^{-1}$, the rate coefficients increase with decreasing energy. This is due to the presence of the zero-energy resonance. However, the nonthermal rate coefficients computed using the MR potential shown in Fig. 9(b) do not display this behavior—the zero-energy resonance simply does not exist for the MR potential. Therefore the ultracold quenching cross sections are very different for the MR and BMP PESs. Nevertheless, both results are in good agreement at $E\sim 100\ \mathrm{cm}^{-1}$, which is expected for high collision energies, since the influence of the zero-energy resonance gradually decreases with energy.

This differs from the strong $j'=8$ contribution from the BMP PES for $\nu<4$ which persists even for higher energies (as demonstrated in Fig. 2). Note further that the j' orderings of the $(\nu=10,j=0)$ state-to-state rate coefficients are not the same as observed for the $(\nu=1,j=0)$ and $(\nu=2,j=0)$ cases.

From these results, we find that the largest discrepancies occurred for vibrational transitions where large changes in angular momentum are allowed. Such transitions probe the anisotropy of the potential to high order. The differences noted for the elastic processes, which are determined by the spherical $(\lambda=0)$ term of the potential, are likely due to improvements made in the BMP PES.

Figures 10(a) and 10(b) display the $(0,2)\rightarrow(0,0)$ and

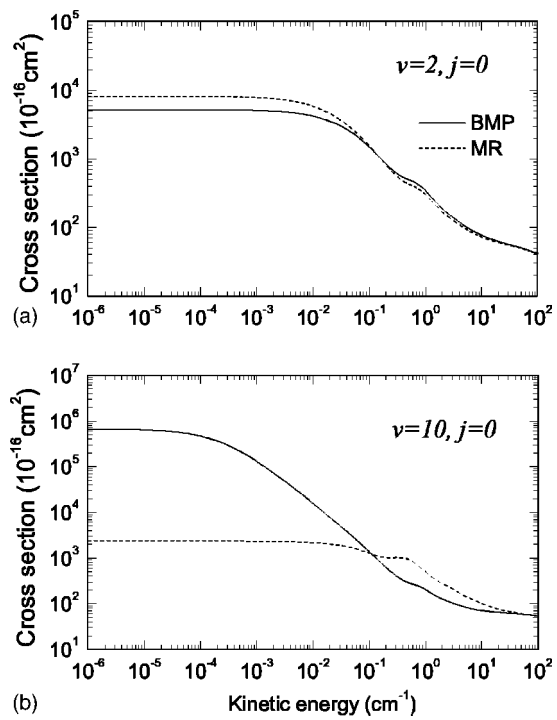

FIG. 8. Elastic cross sections $\sigma_{2,0}$ (a) and $\sigma_{10,0}$ (b) as a function of collision energy. The two potentials again give good agreement for elastic scattering at high collision energies. The presence of a zero-energy resonance for $(\nu=10,j=0)$ causes a significant increase in the BMP result at low energies and a shift in the onset of the Wigner threshold behavior at ultracold energies.

Downloaded 31 Dec 2004 to 146.186.234.236. Redistribution subject to AIP license or copyright, see http://jcp.aip.org/jcp/copyright.jsp

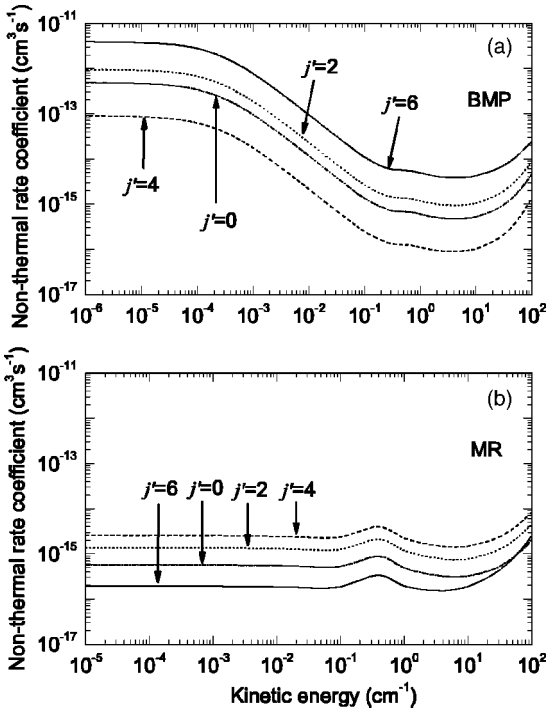

FIG. 9. (a) Inelastic cross section $\sigma_{10,0\to 9,j'}$ times collision velocity (nonthermal rate coefficient) as a function of collision energy computed with the BMP potential. The increase in the cross sections with decreasing energy is due to the presence of a zero-energy resonance. (b) Same as (a) but with the MR potential. There is no zero-energy resonance for the MR potential, so the ultracold results are very different than in (b).

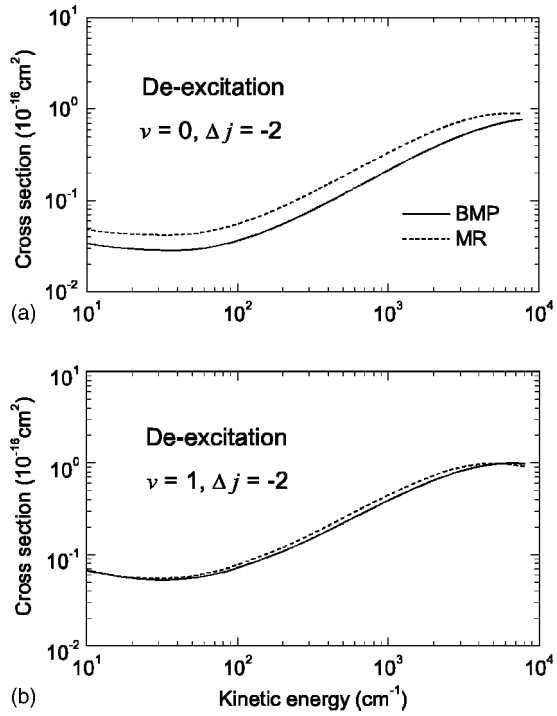

FIG. 10. Comparison of BMP and MR based deexcitation cross section for the $\Delta j=-2$ rotational transition from the $j=2$ initial rotational level of H_2 in vibrational levels of $\nu=0$ and 1 as a function of collision energy.

$(1,2)\to(1,0)$ deexcitation cross sections for pure rotational transitions, respectively. The results from both PESs are very similar, the BMP result is always 10%–30% smaller, the discrepancy being $\sim 10\%$ in the high-energy region. These transitions are not strongly affected by the higher-order anisotropy of the potential (i.e., $\lambda \geqslant 2$), and the BMP results are likely to be improvements. This is further illustrated in Fig. 11 where the zero-temperature total quenching rate coefficients for $\nu=1$ are given as a function of j. For $j>1$, pure rotational quenching dominates and the two PESs give results which agree to within about a factor of 2. The significant drop in the $j=22$ and 23 quenching rate coefficients was explored previously by Forrey.[18]

IV. SUMMARY AND CONCLUSIONS

In summary, we have carefully and critically compared the two most recently published *ab initio* interaction potential energy surfaces (PESs) for HeH_2 by performing elastic and inelastic scattering calculations for collisions of ^{4}He with H_2. The calculations were performed using a nonreactive quantum-mechanical close-coupling method and were carried out for collision energies ranging from the ultracold (10^{-6} cm^{-1}) to the thermal (100 cm^{-1}) regime. Using Muchnick and Russek[21] PES, we have reproduced the inelastic cross sections $\sigma_{10\to 0j'}(E)$ and the total quenching rate coefficients of Balakrishnan *et al.*[15] However, the inelastic cross sections $\sigma_{10\to 0j'}(E)$ obtained from the Boothroyd *et al.*[25] PES are significantly different. The corresponding total quenching rate coefficients turn out to be a thousand times larger than those obtained with the MR surface that agree well with the measurements of Audibert *et al.*[3] We attribute this discrepancy to an enhancement, possibly unphysical, in a high-order anisotropy component of the BMP potential which is manifested primarily in the $(\nu=1,j=0)$ to $(\nu'=0,j'=8)$ transition. The effect, which is a combination of a sizeable overlap of wave functions for transitions between states with a small energy gap and a large anisotropic potential coupling, is observed for the total quenching cross section from other $(\nu,j=0)$ states until the $j'=8$ channel

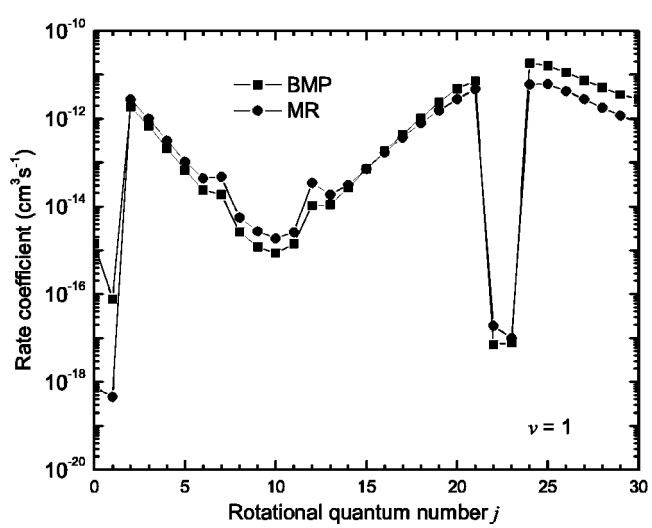

FIG. 11. Zero-temperature total quenching rate coefficients for $\nu=1$ as a function of rotational quantum number j. For $j>1$, pure rotational quenching is allowed and the two potentials give better agreement. The j dependence of the rate coefficients has been explored in detail by Forrey (Ref. 18).

Downloaded 31 Dec 2004 to 146.186.234.236. Redistribution subject to AIP license or copyright, see http://jcp.aip.org/jcp/copyright.jsp

becomes closed. The effect is suppressed when either the energy gap is increased (e.g., by increasing the molecular target reduced mass) or when pure rotational transitions dominate the quenching. These results lead us to postulate, primarily based on the discrepancy with experiment, that the high-order anisotropy components of the BMP potential surface are not accurately determined and make the PES unsuitable for studies of vibrational transitions.

We also find zero-energy resonances in the BMP potential which result in significant enhancements to both the elastic and inelastic cross sections. There are, however, no experimental data which could help to determine the reality of the zero-energy resonances. While the $(\nu=10,j=0)$ elastic cross sections for both PESs agree well at high energies, the results are considerably different at ultracold energies because of the manifestation of the zero-energy resonance for the BMP surface, causing a shift in the onset of the Wigner threshold behavior in this energy regime.

Finally, for pure rotational transitions, the cross sections obtained with the two PESs agree within a factor of 2. This difference may actually signify improvements in the BMP surface for the less anisotropic components of the potential. In conclusion, the BMP surface needs to be reevaluated before it can be adopted in large-scale scattering calculations. Further experiments are needed for inelastic and elastic processes to aid in resolving these issues as well as for benchmarking the scattering calculations.

ACKNOWLEDGMENTS

T.G.L. acknowledges support from the University of Kentucky with additional support from ORNL and the University of Georgia; and general discussions with Dr. Predrag Kristic. The work of C.R., R.M., T.K.C., and R.C.F. was supported by NSF Grant No. PHY-0244066. N.B. acknowledges support from NSF Grant No. PHY-0245019. P.C.S. acknowledges support from NSF Grant No. AST-0087172 and helpful discussions with Stephen Lepp. A.D. was supported by the Chemical Sciences, Geosciences, and Biosciences Division of the Office of Basic Energy Sciences, U.S. Department of Energy.

[1] C. S. Roberts, J. Chem. Phys. **131**, 203 (1963).
[2] J. E. Dove and H. Teitelbaum, Chem. Phys. **6**, 431 (1974).
[3] M. M. Audibert, thèse de Doctorat d'Etat, Université de Paris-Sud, 1976; M. M. Audibert, C. Joffrin, and J. Ducuing, J. Chem. Phys. **61**, 4357 (1974); M. M. Audibert, R. Vilaseca, J. Lukasik, and J. Ducuing, Chem. Phys. Lett. **31**, 232 (1975); **37**, 408 (1976).
[4] J. Lukasik, Chem. Phys. Lett. **44**, 219 (1976).
[5] M. H. Alexander and P. McGuire, J. Chem. Phys. **64**, 452 (1976); M. H. Alexander, *ibid.* **66**, 4608 (1977).
[6] A. W. Raczkowski, W. A. Lester, and W. H. Miller, J. Chem. Phys. **69**, 2692 (1978).
[7] G. D. Billing, Chem. Phys. **30**, 387 (1978).
[8] C. S. Lin and D. Secrest, J. Chem. Phys. **70**, 199 (1979); C. S. Lin, *ibid.* **73**, 1159 (1980).
[9] G. Jolicard and A. Grosjean, J. Chem. Phys. **78**, 2327 (1983).
[10] J. M. Doyle, B. Friedrich, J. Kim, and D. Patterson, Phys. Rev. A **52**, R2515 (1995); J. D. Weinsein, R. deCarvalho, T. Guillet, B. Friedrich, and J. M. Doyle, Nature (London) **395**, 148 (1998).
[11] J. T. Bahns, W. C. Stwalley, and P. L. Gould, J. Chem. Phys. **104**, 9689 (1996); J. T. Bahns, P. L. Gould, and W. C. Stwalley, Adv. At., Mol., Opt. Phys. **42**, 171 (2000).
[12] A. Fioretti, D. Comparat, A. Crubellier, O. Dulieu, F. MasnouSeeuws, and P. Pillet, Phys. Rev. Lett. **80**, 4402 (1998).
[13] T. Takekoshi, B. M. Patterson, and R. J. Knize, Phys. Rev. A **59**, R5 (1999).
[14] N. Balakrishnan, R. C. Forrey, and A. Dalgarno, Chem. Phys. Lett. **280**, 1 (1997); N. Balakrishnan, V. Kharchenko, R. C. Forrey, and A. Dalgarno, *ibid.* **280**, 5 (1997).
[15] N. Balakrishnan, R. C. Forrey, and A. Dalgarno, Phys. Rev. Lett. **80**, 3224 (1998).
[16] R. C. Forrey, N. Balakrishnan, V. Kharchenko, and A. Dalgarno, Phys. Rev. A **58**, R2645 (1998); R. C. Forrey, V. Kharchenko, N. Balakrishnan, and A. Dalgarno, *ibid.* **59**, 2146 (1999).
[17] R. C. Forrey, N. Balakrishnan, A. Dalgarno, M. R. Haggerty, and E. J. Heller, Phys. Rev. Lett. **82**, 2657 (1999); R. C. Forrey, N. Balakrishnan, A. Dalgarno, M. R. Haggerty, and E. J. Heller, Phys. Rev. A **64**, 022706 (2001).
[18] R. C. Forrey, Phys. Rev. A **63**, 051403 (2001); **66**, 023411 (2002).
[19] D. R. Flower, E. Roueff and C. J. Zeippen, J. Phys. B **31**, 1105 (1998).
[20] N. Balakrishnan, R. C. Forrey, and A. Dalgarno, Astrophys. J. **514**, 520 (1999); N. Balakrishnan, M. Vieira, J. F. Babb, A. Dalgarno, R. C. Forrey, and S. Lepp, *ibid.* **524**, 1122 (1999).
[21] P. Muchnick and A. Russek, J. Chem. Phys. **100**, 4336 (1994).
[22] W. Meyer, P. C. Hariharan, and W. Kutzelnigg, J. Chem. Phys. **73**, 1880 (1980).
[23] A. Russek and R. G. Garcia, Phys. Rev. A **26**, 1924 (1982).
[24] D. W. Schwenke, J. Chem. Phys. **80**, 2076 (1988).
[25] A. I. Boothroyd, P. G. Martin, and M. R. Peterson, J. Chem. Phys. **119**, 3187 (2003).
[26] M. S. Child, *Molecular Collision Theory* (Academic, London, 1974).
[27] M. H. Alexander and D. E. Manolopoulos, J. Chem. Phys. **86**, 2044 (1987).
[28] J. M. Hutson and S. Green, MOLSCAT VER. 14 (Distributed by Collaborative Computational Project 6, Daresbury Laboratory, UK Eng. Phys. Sci. Res. Council, 1994).
[29] A. M. Arthurs and A. Dalgarno, Proc. R. Soc. London, Ser. A **256**, 540 (1960).
[30] R. E. Grisenti, W. Schöllkopf, J. P. Toennies, J. R. Manson, T. A. Savas, and M. Stoll, Phys. Rev. A **61**, 033608 (2000); R. E. Grisenti, W. Schöllkopf, J. P. Toennies, G. C. Hargerfeldt, T. Köhler, and M. Stoll, Phys. Rev. Lett. **85**, 2284 (2000).
[31] A. Kalinin, O. Kornilov, and J. P. Toennies, J. Chem. Phys. **121**, 625 (2004).
[32] R. V. Krems, J. Chem. Phys. **116**, 4525 (2002).
[33] R. V. Krems, A. A. Buchachenko, N. Markovíc, and S. Nordholm, J. Chem. Phys. **117**, 166 (2002).
[34] N. Uudus, S. Magaki, and N. Balakrishnan, J. Chem. Phys. (in press).
[35] N. Balakrishnan, G. C. Groenenboom, R. V. Krems, and A. Dalgarno, J. Chem. Phys. **118**, 7386 (2003).
[36] C. Bissonnette, C. E. Chuaqui, K. G. Crowell, and R. J. Le Roy, J. Chem. Phys. **105**, 2639 (1996).
[37] D. W. Schwenke, S. P. Walch, and P. R. Taylor, J. Chem. Phys. **98**, 4738 (1993).
[38] J. C. Flasher and R. C. Forrey, Phys. Rev. A **65**, 032710 (2002).

Downloaded 31 Dec 2004 to 146.186.234.236. Redistribution subject to AIP license or copyright, see http://jcp.aip.org/jcp/copyright.jsp